ACS APPLIED MATERIALS & INTERFACES

Research Article

www.acsami.org

Facile Synthesis of Ag Interlayer Doped Graphene by Chemical Vapor Deposition Using Polystyrene As Solid Carbon Source

Tianru Wu,[†] Honglie Shen,[†,*] Lei Sun,[†] Bin Cheng,[†] Bin Liu,[†] and Jiancang Shen[‡]

[†]College of Materials Science & Technology, Nanjing University of Aeronautics & Astronautics, Nanjing, 211100, China

[‡]National Laboratory of Solid State Microstructure and Department of Physics, Nanjing University, Nanjing, 210093, China

ABSTRACT: Graphene was synthesized by chemical vapor deposition using polystyrene as the solid carbon source. The number of graphene layers could be controlled by regulating the weight of polystyrene under atmospheric pressure at 1000 °C. Silver nanoparticles were then deposited on the graphene by a citrate reduction method. The interaction between graphene and silver was investigated by suface-enhanced Raman scattering spectra and X-ray photoelectron spectroscopy. The change in the G band position indicates n-type doping of the graphene due to an interaction between the silver and the graphene. Silver interlayer doped four-layer graphene shows a sheet resistance of 63 Ω/sq and a light transmittance of 85.4% at 550 nm. The optical and electrical quality of graphene exceeds the minimum industry standard for indium tin oxide replacement materials. It is clearly understood that the environmental sheet resistance stability of the interlayer doped graphene film is better than that of surface doped graphene sheets. The presence of graphene at the surface also acts as a protective layer for the inner silver ions and clusters

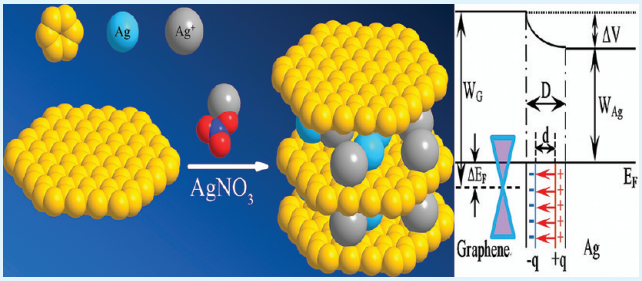

KEYWORDS: *graphene, polystyrene, pressure, monolayer, silver nitrate*

1. INTRODUCTION

Graphene, a single atomic layer of carbon atoms, has stimulated intense research interest because of its unique structure and outstanding properties.[1,2] The considerable research on graphene has motivated the scalable production of high-quality graphene and graphene devices. An ideal monolayer of graphene has a light transmittance of 97.7%, with electron mobility values in excess of 15000 cm^2 V^{-1} S^{-1} at room temperature.[3] Because of the high conductivity and the high light transmittance, graphene is a promising material for flexible transparent conductive electrodes. Recently, growth of graphene using several different methods has succeeded in large area syntheses.[4,5] In particular, large-area monolayer graphene with excellent quality can be synthesized by chemical vapor deposition (CVD) with a controllable thickness range of layers for possible application as transparent conductive electrodes.[6] Recently, Li et al reported that four layers of graphene have the sheet resistance of 350 Ω/sq and light transmittance of 90%.[7] However, their sheet resistances were still higher than those of carbon nanotube-based transparent conductive electrodes and indium tin oxide (ITO).[8] The optical and electrical quality of graphene strongly depends on the growth conditions, and low sheet resistance could be realized by improving the crystallinity and reducing the densities of defects and wrinkles in graphene.[9]

Recently, the main strategies for improving the electrical conductivity of graphene films have been launched on various doping treatments.[10,11] The interaction between graphene and metal was investigated.[12] The layer number of graphene was found to affect the morphology of the metal deposited graphene and the chemical reactivity of graphene.[13] In addition, the optical and electronic properties of the graphene sheets are extremely sensitive to the interaction between metal and graphene.

In this article, graphene with good structure and optical performance was synthesized by CVD on Cu foil using solid polystyrene precursor for cost reduction and practical application. Compared to other solid or liquid carbon source, polystyrene was found to be a perfect precursor to grow high-quality graphene, because it could be decomposed into styrene, which contains benzene, a ring-structured molecule and resembles the basic unit of graphene. Meanwhile, polystyrene does not contain potential topological defect generators and concentrations of heteroatoms, such as oxygen, nitrogen, sulfur, etc. After different layers of graphene was synthesized by controlling the weight of solid precursor, it was found that using Ag chemical doping is an easy way to improve the conductivity of transparent graphene. Ag nanoparticles were synthesized on the graphene sheets by $AgNO_3$ reduction method. The interaction between Ag and graphene was more prominent in the case of interlayer doped graphene than that of surface doped graphene. The Ag deposition on graphene can induce n-type doping effect. By adopting the interlayer doping method, the lowest sheet resistance of 63Ω/sq with 85.4% light

Received: January 3, 2012
Accepted: March 30, 2012
Published: March 30, 2012

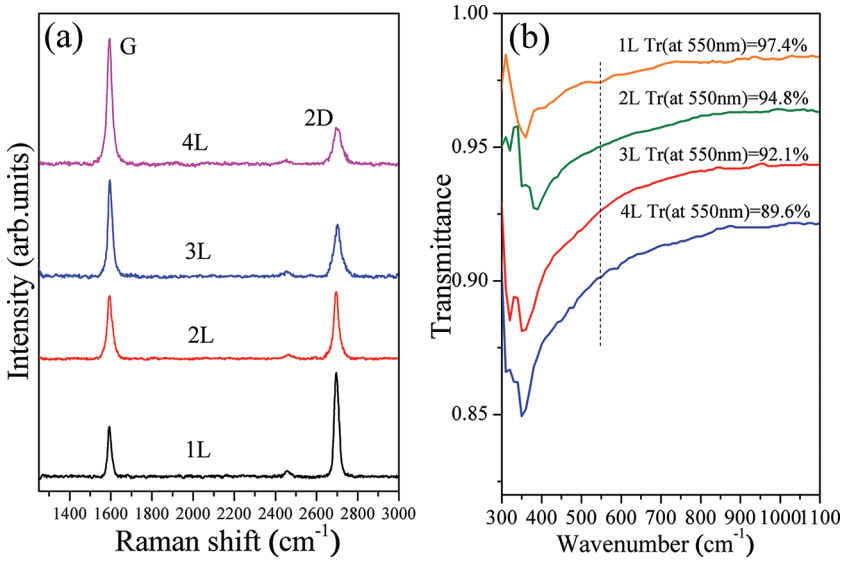

Figure 1. (a) Raman spectra of SLG ang FLG; (b) UV−vis spectra of single and few layer transferred grapheme films on quartz substrates.

transmittance was obtained, which is comparable to those of ITO films (R_s = 20−50 Ω/sq, Trans = 85−90%). Therefore, preparation of Ag interlayer doped graphene by solid precursors at low cost will be attractive for industrial production such as photovoltaic devices.

2. EXPERIMENTAL SECTION

In this study, graphene syntheses under different conditions were performed using hydrogen and argon gas mixture and polystyrene as a solid precursor. The solid precursor loaded in a small quartz tube with one side sealed was placed at the gas influx side of the quartz tube. Before synthesis, the 50 μm thick Cu foil substrate was roughly polished with metal polish paste, and then was electropolished to form a smooth Cu face. The Cu foil was inserted into the quartz tube and then was annealed at 1035 °C under a mixture of H_2 and Ar gas flow for 30 min. The purpose of annealing is to initiate Cu grain growth, to remove residual copper oxide and smooth the surface.[14] The solid-state polystyrene was subsequently heated to about 280 °C by a heating lamp under a mixture of H_2 and Ar gas flow. The weight of solid precursor is an efficient way to control the number of layers. 1−4 layer graphene sheets were synthesized by regulating the weight of polystyrene (15, 35, 50, and 70 mg) with Ar (300 sccm) and H_2 (100 sccm) gas flow under atmospheric pressure at 1000 °C for 30 min. After growth process, the furnace and heating lamp were turned off and the whole furnace was cooled down to room temperature naturally.

Single-layer graphene (SLG) and few-layer graphene (FLG) sheets were transferred onto SiO_2/Si and quartz substrates. A layer of polymethyl methacrylate (PMMA) (MicroChem, 950,000 MW, 5−10 wt.% in anisole) was spin coated on the graphene/Cu layer. The Cu foil substrate was removed by electrochemical reaction with aqueous 0.1 M ammonium persulphate solution $(NH_4)_2S_2O_8$.[15] After placing the PMMA/graphene stack on the target substrate, the PMMA/graphene/substrate stack was heated at 170 °C for 30 min to ensure a close bonding of the graphene to the substrate. The PMMA was then removed by anisole, acetone and deionized water, and graphene/substrate stack was annealed at 450 °C for 90 min under hydrogen (700 sccm) and argon (300 sccm) to remove the residual PMMA.[16] Finally, the graphene films were then immersed into a H_2O_2 solution (30%) for over 10 h to remove the amorphous carbon impurities and to obtain a hydrophilic surface.[17]

For surface doped graphene, Ag nanoparticles (AgNPs) were formed on the surface of the SLG and FLG by a citrate reduction method.[18] 0.2 g of silver nitrate ($AgNO_3$) (99%, Aladdin) was dissolved in 100 mL of deionized water. SLG or FLG on SiO_2/Si and quartz substrate was immersed into the solution and was kept at about 60−90 °C for 10−20 min. During the process of citrate reduction, 5 mL of 1% sodium citrate solution was added drop by drop and the solution was mixed slowly. For interlayer doped graphene, SiO_2/Si substrate was first immersed into the silver nitrate solution as mentioned above. A fresh graphene layer is then transferred onto the SiO_2/Si substrate and immersed into the silver nitrate solution again. This step was repeated several times on the same graphene transferred substrate in order to achieve interlayer doped graphene sheets up to four layers. It is well-known that melting point of small nanometre-size particles differs from that of bulk materials. The Ag nanoparticles used (20−40 nm) exhibited obvious sintering behavior at significantly lower temperatures (150 °C-250 °C) than the T_{melt} (960 °C) of silver.[19] To avoid the aggregation and volatilization of Ag nanostructures at high temperature, the transferred graphene sheet should be kept without undertaking the anneal process under hydrogen and argon after the PMMA was removed by anisole, acetone and deionized water. For comparison, HNO_3 interlayer doped graphene layers and Ag surface doped graphene layers were also fabricated. A nitric acid solution of 20% in deionized water was used as NO_3^- dopant of graphene sheet. The technological process of HNO_3 interlayer doped graphene was the same as that of $AgNO_3$ interlayer doped graphene.

Raman microprobe spectroscopy (Horiba JY T64000-UH) using an Ar^+ laser (wavelength 514.5 nm) with a 1 μm laser spot, equipped with an optical reflectance microscopy, was used to evaluate the crystalline quality of the samples. Transmission/reflection microscopy (Shanghai Changfang Optical Instrument Co., Ltd.CMM-50) and Scanning electron microscopy (SEM, LEO 1530VP) with operating voltage of 5 kV was used to characterize the morphology of the graphene sheets. The samples were characterized by atomic force microscope (AFM, Park System XE-120, contact mode). The optical transmission (T) was measured by the Shimadzu UV-2550 spectrophotometer in the 300−1600 nm range. X-ray photoelectron spectroscopy (XPS) analyses were performed on the deposited films using PHI550 ESCA/SAM equipment with a residual pressure of 1×10^{-9} Torr.

3. RESULTS AND DISCUSSION

In the present work, graphene was synthesized by CVD using polystyrene. Polystyrene was chosen as an appropriate precursor to grow high-quality graphene comparing to other solid and liquid precursors. At high temperature, Styrene molecules decomposed by polystyrene just need to dehydrogenate, dissociate and connect to each other to form the graphene structure. The weight of solid precursor is an efficient way to control the number of layers. Raman analysis of

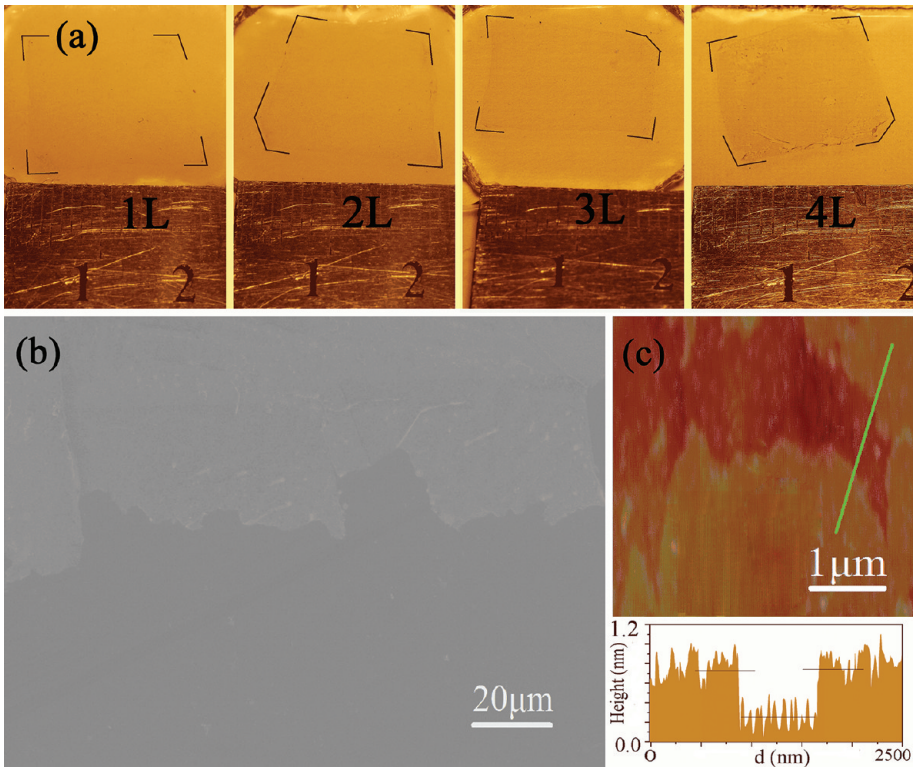

Figure 2. (a) Optical images for the monolayer, bilayer, trilayer, and four-layer samples of transferred graphene layers. (b) SEM image of the edge of graphene sheet transferred onto SiO_2/Si. (c) AFM image of monolayer graphene and the height of graphene sheet.

graphene in Figure 1(a) was performed to ascertain the typical features and quality of graphene sheets synthesized under different process conditions. It was found that SLG and FLG could be synthesized under ambient pressure by regulating the weight of solid precursors. Two prominent graphene peaks appeared in the Raman spectra at ~1582 and ~2700 cm^{-1}, corresponding to G and 2D bands. D band (~1350 cm^{-1}), a measure of defects in the graphene, is absent in the Raman spectra, demonstrating the high quality of the graphene films synthesized by polystyrene. Light transmittance and optical micrographs of the transferred SLG and FLG on quartz substrates are shown in Figure 1b and Figure 2a. We can observe the graphene films with good macroscopic uniformity. This result also indicates that the weight of solid precursor is a critical factor to control the number of graphene layers. The densities and motions of the active radicals play a critical role in the overall synthesis of the monolayer graphene. For nucleation of graphene, it has to overcome an energy barrier (ΔG^*) to form a crystal from carbon related radicals, which companied by a decrease of free energy and occurs spontaneously. Once a large supersaturation is achieved, spontaneous nucleation and initial growth of graphene grains occur.[20] Meanwhile, it was found that the use of a very flat, electropolished Cu catalyst surface and low concentration of carbonaceous radicals enables the growth of more uniform and better quality graphene film.[21] After electropolishing and high temperature annealing, the roughness of the graphene/Cu surface is reduced obviously. Figure 2b shows the SEM image of the edge of graphene sheet transferred onto SiO_2/Si. By reducing the roughness and crystal defect of Cu foils by means of polishing and high temperature annealing, we were able to obtain SLG samples with high uniformity and low defects. The theoretical height of a monolayer graphene was approximately 0.36 nm.[22] The corresponding AFM image (shown in Figure 2c) at the edge indicates the height of graphene (~0.57 nm).

After SLG and FLG with good structure and optical performance were synthesized by solid carbon source, Ag was used to dope the graphene films and the sheet resistance was reduced by 70% depending on $AgNO_3$ doping concentration. The diagram of Ag interlayer doping was shown in Figure 3(a). Mechanism of the reaction could be expressed as follows: $4Ag^+ + C_6H_5O_7Na_3 + 2H_2O \rightarrow 4Ag^0 + C_6H_5O_7H_3 + 3Na^+ + H^+ + O_2\uparrow$.[23] The sizes of the Ag particles are less than 15 nm (see Figure 3b, c). After doping with 2 g/L $AgNO_3$, the AgNPs were uniformly formed on the graphene sheet. Then another graphene layer was transferred directly onto that layer. To understand the doping effect, the sample was characterized by Raman spectroscopy. The interaction between graphene and Ag was investigated by studying the surface-enhanced Raman scattering (SERS) spectra of graphene. We defined I_{SERS} and I_{NORMAL} as the intensities of G band calculated from SERS and normal Raman spectra. The I_{SERS}/I_{NORMAL} ratios of G band are 3.2 for single-layer (Figure 4a), 2.3 for bilayer (Figure 4b), 1.7 for trilayer (Figure 4c) and 1.4 for four layers (Figure 4d). The doping effect of graphene with Ag deposition was investigated from changes in the I_{SERS}/I_{NORMAL} ratios and shifts of the G and 2D band (shown in Figure 4(f)). The largest enhancement factor in single-layer graphene is thought to be due to the interaction between Ag and graphene. It is well-known that the peak position of G and 2D band changes depending on the doping effect. The upshift of the G band position and the downshift of the 2D band position means n-doping of graphene, whereas the upshift of the G band position and the upshift of the 2D band position means p-doping due to the phonon stiffening effect by charge extraction.[24] It was noticed the G and 2D bands of the graphene sheet drastically upshifted

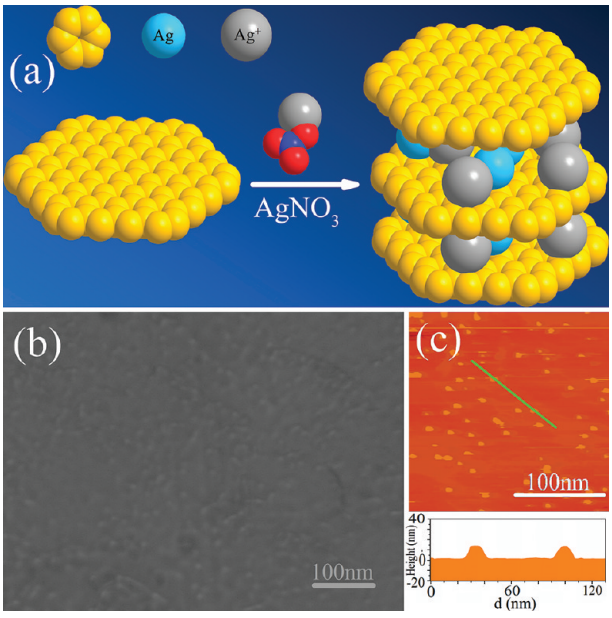

Figure 3. (a) Diagram of Ag interlayer doping. (b) SEM image for Ag interlayer doped four layer graphene. The bright spots indicate the reduced Ag nanoparticles. (c). AFM image of Ag nanoparticles formed on graphene sheet.

after thermal annealing at high temperature.[25] To evaluated and characterize the doping effect of Ag/Ag^+, PMMA on pristine graphene/substrate stack was also be removed by anisole, acetone, and deionized water without the annealing process. For Ag-doped monolayer graphene, the G band shifted about ~6 from ~1587 cm^{-1} (pristine graphene) to ~1593 cm^{-1} (Ag-doped graphene) and the 2D band shifted about ~2 cm^{-1} from ~2685 cm^{-1} (pristine graphene) to ~2683 cm^{-1} (Ag -doped graphene), which means n-type doping of graphene. In particular, the shift of G and 2D band also decreased with increasing the number of graphene layers by surface doping, indicating the strongest interaction occurs between Ag and single-layer graphene (shown in Figure 4f). The peak upshift of G band (~7.5 cm^{-1}), peak downshift of 2D band (~3 cm^{-1}) and I_{SERS}/I_{NORMAL} (~3.5) was more prominent in the case of interlayer doped four-layer graphene doping (Figure 4(f)) than that of surface doped four-layer graphene. Therefore, Ag interlayer doped graphene was adopted to enhance the interaction between Ag and graphene by an electron transfer driven by the work function difference.[26] The strongest interaction occurs among Ag and graphene interlayer stacks. When the Ag metallic nanostructures is excited by electromagnetic radiation, the conductive electronic oscillations result in surface plasmon resonance (SPR) and produce surface plasmons (SPS) spread along the interlayer Ag nanoparticles.

In addition to SERS, binding of metal to graphene is also important for the research on the interaction between graphene and metal. The Ag interlayer doped four layers graphene was investigated by XPS for analysis of the influence of graphene sheets on the SPR properties of Ag nanoparticles, as shown in Figure 5. Two bands at 367.5 and 373.5 eV, ascribed to Ag $3d_{5/2}$ and Ag $3d_{3/2}$ binding energies for bulk Ag are indicated in the figure. The Ag $3d_{5/2}$ and Ag $3d_{3/2}$ peaks shift to higher binding energies at 368.1 and 374.2 eV for Ag deposited on graphene sheet. The deconvolution of these two bands shows peaks at 368.1, 369.5 eV, 374.2 and 375.5 eV, respectively. Those at 368.1 and 374.2 eV could be ascribed to the Ag^+, while those at 369.5 and 375.5 eV are ascribed to Ag^0, all of which display nearly 0.6 eV shift to higher binding energy as a result of electron transfer from metallic Ag to the graphene sheet (see Figure 5). It is originated from the shift in the initial-state potential of ionic charge and the lattice potential. Since the work function of Ag (4.2 eV) is smaller than that of graphene (4.8 eV), electron transfer from the Ag to graphene sheets would occur during the formation of the Ag/graphene heterostructures. Although the bonding is weak, the Ag structures cause the Fermi level to shift upward the conical points in graphene. It further verifies that Ag^0/Ag^+ based

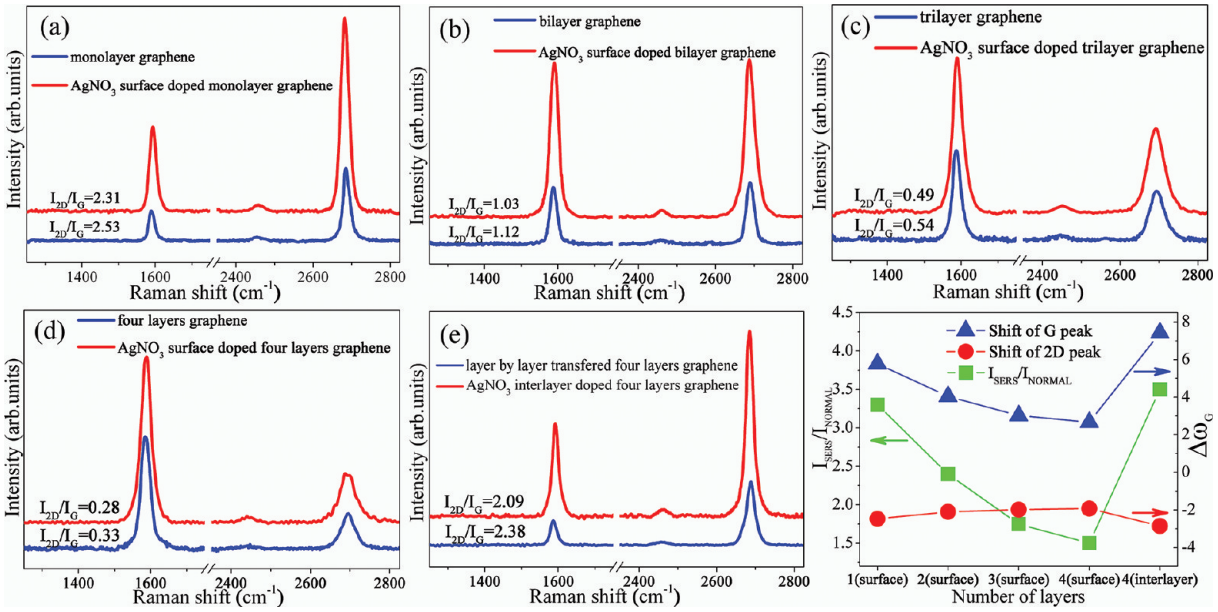

Figure 4. Raman spectra of (a) monolayer, (b) bilayer, (c) trilayer, (d) four-layer, and (e) four layer-by-layer transferred graphene before and after Ag deposition. (f) Enhancement factors of G band calculated from intensities of SERS and normal Raman spectra and the shift of G and 2D bands ($\Delta\omega$) before and after Ag deposition as a function of the layer number of graphene.

dx.doi.org/10.1021/am300014c | ACS Appl. Mater. Interfaces 2012, 4, 2041−2047

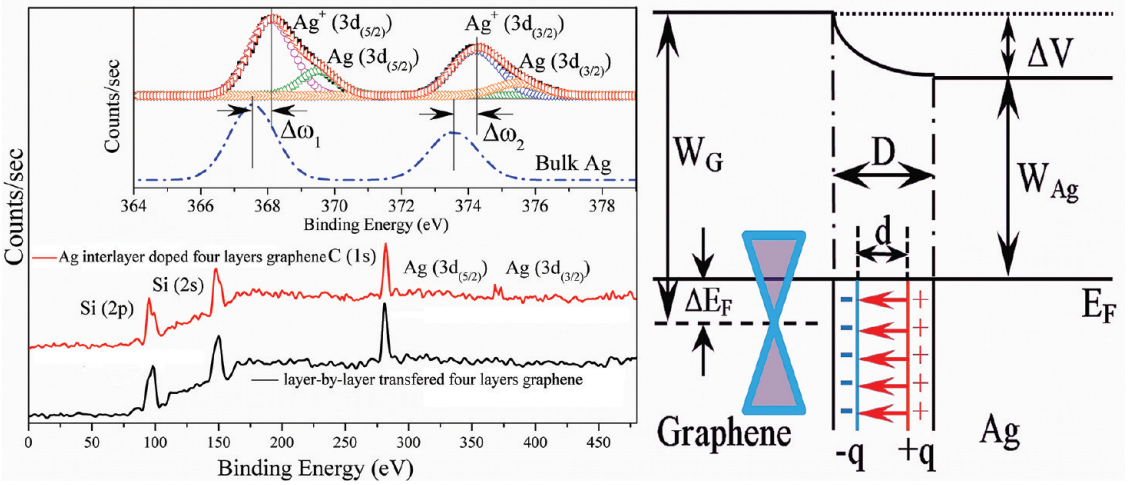

Figure 5. Left one is XPS spectra of Ag interlayer doped graphene. The inset shows Ag $3d_{5/2}$ and Ag $3d_{3/2}$ XPS spectra of bulk Ag and Ag/graphene heterostructures. The right one shows the illustration of energy diagram of the Ag/graphene interface and potential step formation at the graphene–metal interface.

nanoparticles and graphene sheets might serve as electron donor and electron acceptor, which induced n-type doping.

The optical and electronic properties of the graphene sheets are extremely sensitive to the interaction between Ag and graphene and the intensity of SPR. Deposition of inorganic nanoparticles, such as metals or semiconductors, onto graphene sheets would present special features and be useful in optical and electronic devices, catalysis, sensors, and so on. Figure 6

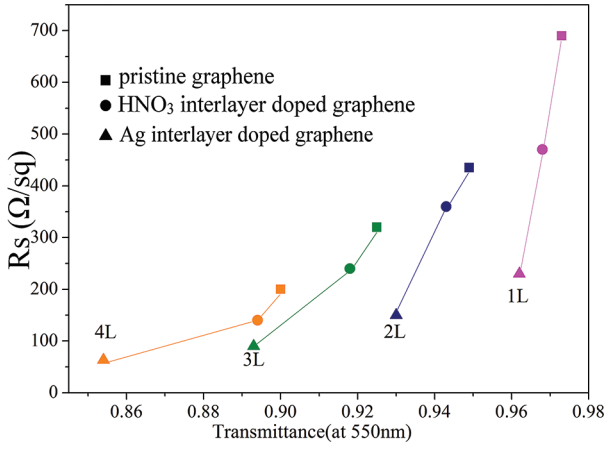

Figure 6. Sheet resistance and light transmittance of pristine, HNO_3-doped, and Ag-doped graphene layers.

shows the sheet resistance and light transmittance of the pristine, HNO_3 interlayer doped graphene and Ag interlayer doped graphene as a function of different layer. The pristine single graphene sheet shows a large sheet resistance of 690 Ω/sq with a light transmittance of 97.3% at 550 nm. Whereas the sheet resistance of Ag interlayer doped four layer graphene reached 63 Ω/sq and a light transmittance of 85.4%, which is comparable to those of indium tin oxide conducting film. The light transmittance of Ag doped graphene slightly decreased due to the light scattering from AgNPs formed during the reduction reaction.[27] Larger interlayer distance of AgNPs interlayer doped graphene is another cause of small optical conductivity.[28] It was also found that $AgNO_3$ concentration was a critical factor, to which the optical and electronic properties is sensitive. The light transmittance of interlayer doped graphene sheets at 2 g/L $AgNO_3$ concentration decreased by only about 5%, while the R_s reduced by 70%. The light transmittance dramatically reduced by 14% at 6 g/L $AgNO_3$ concentration due to the light absorption on the AgNPs but the change of the sheet resistance was similar to that of the 2 g/L $AgNO_3$ concentration.

To analyze light transmittance and sheet resistance data for transparent conductive films, it is important to note that R_s and T are associated. Both are determined by the response of electrons to either static (voltage) or dynamic (light) electric fields.[29] The sheet resistance is ultimately controlled by the (3-dimensional) DC conductivity (σ_{DC}) and is calculated by $R_s = (\sigma_{DC}t)^{-1}$, where t is the film thickness.[30] The light transmittance is controlled by the optical conductivity (σ_{op})[31] and is calculated by $T = (1 + (Z_o/2_{Rs})(\sigma_{op}/\sigma_{DC})^{-2}$, where Z_0 is the impedance of free space and has the value 377Ω. High values of σ_{DC}/σ_{op} result in the desired properties (high T, low R_s). Figure 7 shows the calculated σ_{DC}/σ_{op} values for Ag0doped graphene films. The σ_{DC}/σ_{op} values of pristine and HNO_3 interlayer

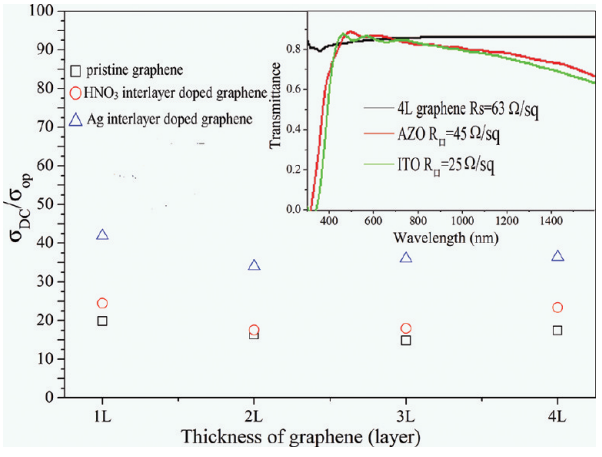

Figure 7. Mean σ_{DC}/σ_{op} values of pristine, HNO_3-doped, and Ag-doped graphene. The inset shows the light transmittance of ITO, AZO, and Ag-doped graphene films on quartz in the 300–1600 nm range.

dx.doi.org/10.1021/am300014c | ACS Appl. Mater. Interfaces 2012, 4, 2041–2047

doped graphene films are also listed for comparison. The mean σ_{DC}/σ_{op} value increases obviously by interlayer Ag doping, showing the high values of 30−40, in contrast to the values of 10−20 for pristine graphene and 20−30 for HNO_3 interlayer doped graphene. The σ_{DC}/σ_{op} value of Ag interlayer doped graphene approaches to the minimum industry standard (σ_{DC}/σ_{op} = 30) for indium tin oxide replacement materials.[32] These results enable us to fabricate highly transparent conducting electrodes, with Ag interlayer doped graphene using solid precursors. The light transmittance of ITO, Al-doped ZnO (AZO) and Ag interlayer doped graphene are shown in Figure 7. Comparing with TCO electrodes which have typical sheet resistance of 15−50 Ω/sq and light transmittance of ∼85% in the visible range (400−900 nm),[8] the Ag doped graphene electrodes have a higher light transmittance in the visible to IR region and are more robust under bending. These techniques are effective for industrial application which excellent optical and electrical performance at relatively low cost and large area production of flexible transparent conductive electrodes.

On the other hand, the AgNPs doping stability was studied. It is clearly understood that the environmental R_s stability of the interlayer doped graphene film is better than that of surface doped graphene sheets. There could be several reasons for this difference. The diameter of Ag ion (1.26 Å) and Ag (1.34 Å) are larger than the diameter of a benzene ring (1.05 Å). Therefore, Ag ions and clusters are unlikely to penetrate through the graphene layer except the cracks, domain boundaries and defects.[33] The penetrated Ag ions and clusters still remain unchanged because the graphene is already doped and saturated. The presence of graphene at the surface also acts as a protective layer for the inner Ag ions and clusters. So Ag interlayer doping is considered to be an efficient approach to producing graphene sheets with good flexibility, transparency, and low cost needed for industrial application such as organic solar cells.

4. SUMMARY

Here we introduced an effective and low-cost method for fabrication of Ag interlayer doped graphene by CVD using polystyrene. After one and few layers of graphene with good uniformity and optical performance were synthesized by controlling the weight of solid precursor, the interaction between Ag and different layers of graphene was investigated. Ag interlayer doped graphene showed a larger Raman signal compared to those of surface doped graphene, indicating the enhancement of the interaction between Ag and graphene. Furthermore, the Ag deposition on graphene can induce n-type doping of graphene. Ag^0/Ag^+ based nanoparticles and graphene sheets serve as electron donor and electron acceptor. The Ag/graphene heterostructures cause the Fermi level to shift upward from the conical points in graphene due to the work function difference of Ag (4.2 eV) and graphene (4.8 eV), which induced n-type doping.

The new method of interlayer Ag doping was also developed to decrease the sheet conductivity of grapheme films and to improve environmental stability. The optimized Ag doped four-layer graphene shows a sheet resistance of 63 Ω/sq and a light transmittance of 85.4% at 550 nm with excellent stability. Because of the low cost solid carbon source and Ag doping technics, the CVD process enables inexpensive and efficient syntheses of high-quality graphene films over large areas, which will be helpful in facilitating a wide range of cost reduction and practical application of graphene.

AUTHOR INFORMATION

Corresponding Author

*Tel: 86-25-52112901. Fax: 86-25-52112626. E-mail: hlshen@nuaa.edu.cn.

Notes

The authors declare no competing financial interest.

ACKNOWLEDGMENTS

This work is performed with a financial support from the National Natural Science Foundation of China (61176062) and the project funded by the Priority Academic Program Development of Jiangsu Higher Education Institutions.

REFERENCES

(1) Huang, X.; Qi, X. Y.; Boey, F.; Zhang, H. *Chem. Soc. Rev.* **2012**, *41*, 666.
(2) Huang, X.; Yin, Z.; Wu, S.; Qi, X.; He, Q.; Zhang, Q.; Yan, Q.; Boey, F.; Zhang, H. *Small* **2011**, *7*, 1876−1902.
(3) Kim, K. S.; Zhao, Y.; Jang, H.; Lee, S. Y.; Kim, J. M.; Kim, K. S. *Nature* **2009**, *457*, 706−711.
(4) Cao, X.; Shi, Y.; Shi, W.; Lu, G.; Huang, X.; Yan, Q.; Zhang, Q.; Zhang, H. *Small* **2011**, *7*, 3163−3168.
(5) Huang, P. Y.; RuizVargas, C. S.; Zande, A. M.; Whitney, W. S.; Levendorf, M. P.; Kevek, J. W. *Nature* **2011**, *469*, 389−392.
(6) Li, X.; Magnuson, C. W.; Venugopal, A.; An, J.; Suk, J. W.; Han, B. *Nano Lett.* **2010**, *10*, 4328−4334.
(7) Li, X.; Zhu, Y.; Cai, W.; Borysiak, M.; Han, B.; Chen, D. *Nano Lett.* **2009**, *9*, 4359−4363.
(8) Kim, H.; Horwitz, J. S.; Kushto, G.; Pique, A.; Kafafi, Z. H.; Gilmore, C. M.; Chrisey, D. B. *J. Appl. Phys.* **2000**, *10*, 886021.
(9) Lin, Y. C.; Jin, C.; Lee, J. C.; Jen, S. F.; Suenaga, K.; Chiu, P. W. *ACS Nano* **2011**, *5*, 2362−2368.
(10) Bae, S.; Kim, H.; Lee, Y.; Xu, X.; Park, J. S.; Zheng, Y. *Nat. Nanotechnol.* **2010**, *5* (8), 574−578.
(11) Wang, S. J.; Geng, Y.; Zheng, Q. B.; Kim, J. K. *Carbon* **2010**, *48* (6), 1815−1823.
(12) Pollak, E.; Geng, B.; Jeon, K. J.; Lucas, I. T.; Richardson, T. J.; Wang, F. *Nano Lett.* **2010**, *10*, 3386−3388.
(13) Ling, X.; Xie, L. M.; Fang, Y.; Xu, H.; Zhang, H. L.; Kong, J. *Nano Lett.* **2010**, *10*, 553−561.
(14) Li, X.; Magnuson, C. W.; Venugopal, A.; Tromp, R. M.; Hannon, J. B.; Vogel, E. M. *J. Am. Chem. Soc.* **2011**, *133*, 2816−2819.
(15) Sukang, B.; Hyeongkeun, K.; Youngbin, L.; Xiangfan, X.; JaeSung, P.; Yi, Z. *Nat. Nanotechnol.* **2010**, *5*, 574−578.
(16) Lin, Y. C.; Lu, C. C.; Yeh, C. H.; Jin, C. H.; Suenaga, K.; Chiu, P. W. *Nano Lett.* **2012**, *12*, 414−419.
(17) Xinming, L.; Hongwe, Z.; Kunlin, W.; Anyuan, C.; Jinquan, W.; Chunyan, L. *Adv. Mater.* **2010**, *22*, 2743−2748.
(18) Daming, C.; Qinghua, X. *Chem. Commun.* **2007**, *14*, 248−250.
(19) Moon, K. S.; Dong, H.; Maric, R.; Pothukuchi, S.; Hunt, A.; Li, Y.; Wong, C. P. *J. Electron. Mater.* **2005**, *34*, 168−175.
(20) Wu, W.; Yu, Q. K.; Peng, P.; Liu, Z. H.; Bao, J. M.; Pei, S. S. *Nat. Nanotechnol.* **2012**, *23*, 356−361.
(21) Zheng, L.; Ye, L.; Daniel, W.; Singer, J.; Matthew, E.; Berck, L. A. *Chem. Mater.* **2011**, *23*, 1441−1447.
(22) Mcallister, M. J.; Lio, J. L.; Adamson, D. H.; Schniepp, H. C.; Abdala, A. A.; Liu, J.; et al. *Chem. Mater.* **2007**, *19*, 4396−404.
(23) Zheng, Q. B.; Lin, X. Y.; Nariman, Y.; Yeung, K. K.; Li, Z. G.; Kim, J. K. *ACS Nano* **2011**, *5* (7), 6039−6051.
(24) Pisana, S.; Lazzeri, M.; Casiraghi, C.; Novoselov, K. S.; Geim, A. K.; Ferrari, A. C.; Mauri, F. *Nat. Mater.* **2007**, *6*, 198−201.
(25) Cheng, Z. G.; Zhou, Q.; Wang, C. X.; Li, Q.; Wang, C.; Fang, Y. *Nano Lett.* **2011**, *11*, 767−771.
(26) Giovannetti, G.; Khomyakov, P. A.; Brocks, G.; Karpan, V. M.; Brink, J.; Kelly, P. *J. Phys. Rev. Lett.* **2008**, *101*, 026803.

(27) Kim, K. K.; Bae, J. J.; Park, H. K.; Kim, S. M.; Geng, H. Z.; Park, K. A.; Shin, H. J.; Yoon, S. M.; Benayad, A.; Choi, J. Y. *J. Am. Chem. Soc.* **2008**, *130*, 12757−12761.
(28) De, S.; Coleman, J. N. *ACS Nano* **2010**, *4*, 2713−2720.
(29) Li, X.; Zhu, Y.; Cai, W.; Borysiak, M.; Han, B.; Chen, D.; Piner, R. D.; Colombo, L.; Ruoff, R. S. *Nano Lett.* **2009**, *9*, 4359−4363.
(30) Cai, W. W.; Zhu, Y. W.; Li, X. S.; Piner, R. D.; Ruoff, R. S. *Appl. Phys. Lett.* **2009**, *95*, 123115.
(31) Peter, N. N.; Philip, E. L.; Sukanta, D.; Jonathan, N.; Coleman, N.; John, J. B. *Nano Lett.* **2009**, *9*, 3890−3895.
(32) Libo, G.; Wencai, R.; Jinping, Z.; Laipeng, M.; Zongping, C.; Huiming, C. *Appl. Phys. Lett.* **2010**, *97*, 183109.
(33) Dong, X.; Fu, D.; Fang, W.; Shi, Y.; Chen, P.; Li, L. J. *Small* **2009**, *5*, 1422−1426.